Transport Properties of $Ge_{1-x}Mn_xSe$ System

N. Makram and L.A. Wahab*

Faculty of Science (Girls), El-Azhar University, Cairo, Egypt.
**National Center for Radiation Research and Technology, Nasr City, Cairo, Egypt.*

Study of the ac and dc conductivities of semimagnetic semiconductor $Ge_{1-x}Mn_xSe$ (x = 0.1 and 0.2) has been carried out. The activation energy and the pre-exponential factor which appear in the dc conductivity are found to decrease with increasing Mn. The dielectric response and ac conductivity of the samples are investigated in the frequency range from 50 Hz to 5 MHz and temperature range from 300 to 420 K. The obtained data reveal that $s_{ac}(w)$ obey the relation $s_{ac}(w) = A\ w^s$, and the exponent s was found to be » 1. The analysis of results shows that the dominant conduction mechanism follows the quantum mechanical tunneling (QMT). The ESR spectra showed that the investigated samples are paramagnetic materials at room temperature. The calculated number of defects illustrates that with increasing Mn the number of defects increases. The magnetic properties are determined by the measurement of magnetization as a function of magnetic field. The results indicated the paramagnetic behavior for x = 0.1. While as x increased to 0.2 the results indicated the ferromagnetic exchange interaction between the magnetic ions.
Keywords: Transport Properties, Magnetic Properties and Semimagnetic Semiconductors.

1. Introduction:

Diluted magnetic semiconductors (DMS), often referred to as semimagnetic semiconductors, that are based on (III-V) and (II-VI) semiconductors doped with magnetic materials have attracted a great deal of attention recently because of their potential applications in spintronic devices that exploit the charge and spin of electrons[1]. The lattice of these materials consist of magnetic ions partially substituting for some of the cations, thereby including a local magnetic moment in the lattice, and donating carriers into the system. Semiconductors are used for information processing and communication, whereas magnetic materials are used for recording information. These operations can theoretically be done simultaneously in magnetic semiconductors devices. Moreover, it is possible to inject spin–polarized current into semiconductors to

control the spin states of carriers. This is one of the quantum bit operations required for quantum computing [2]. Sources of spin-polarized carriers integrated in both light-emitting diodes and resonant tunneling diode heterostructures have been built using this technology [3,4].

Typical magnetic semiconductors are Mn–doped wide band gap semiconductors such as $II_{1-x}Mn_xVI$, $III_{1-x}Mn_xV$, $IV_{1-x}Mn_xIV$ and some of oxide systems like Co – doped ZnO [5-9]. Mn doped DMS are important semiconducting materials due to their applications in magneto optics, spintronics, displays, and lasers [10]. Mn^{2+} has a relatively large magnetic moment (S=5/2) due to $4S^0$ $3d^5$ electronic configuration in its outer shell. In such materials, large S-d exchange interaction between magnetic ions and electrons in valence band can lead to unusual electronic, optical and magneto – optical properties.

In the present work preparation and characterization of $Ge_{1-x}Mn_xSe$ (x = 0.1 and 0.2) compounds were considered. Study of structure by scanning electron microscope (SEM) and X-ray diffraction has been carried out. Dependence of dc and ac conductivities on temperature and frequency are investigated. Detection of defects has been carried out using electron spin resonance (ESR). The magnetic properties were studied at room temperature.

2. Experimental:

The $Ge_{1-x}Mn_xSe$ (x = 0.1 and 0.2) semimagnetic semiconductor materials were prepared by the melting quenching technique. Appropriate amount of Ge, Mn and Se elements of 5N nominal purity were sealed in evacuated ampoules and then placed in furnace whose temperature was raised gradually and kept constant for 2h at 500 ^{0}C, then raised to 1000^{0}C for 25h. During this period the molten was occasionally shaken to ensure homogeneous mixing of the constituents. The molten was then rapidly quenched in a mixture of water and ice. The chemical examination of the prepared samples was carried out by the energy dispersive X-ray analysis (EDX) using apparatus model Joel 6400. The EDX data confirms the presence of the elemental ratio as prepared according to the atomic weight of each element within an accuracy of ± 0.02, as shown in Fig.(1). The structure was studied by X-ray powder diffraction XRD using Shimadzu X-ray, with Cu K_α tube. The surface morphology of the studied samples was examined using the scanning electron microscope.

Samples for electrical measurement were prepared in the form of discs of thickness ≈ 0.2 cm. Good contact was achieved through two coaxial carbon- dag electrodes of ≈ 2 mm diameter applied to opposite faces of the disc. The dc

conductivity was measured as a function of temperature using oxford cryostat connected to 617 Keithley electrometer over the temperature range 300-420 K. The LCR bridge model Hioki 3532 LCR Hitester was used to measure the AC conductivity of the samples in the frequency range from 50 Hz – 5MHz.

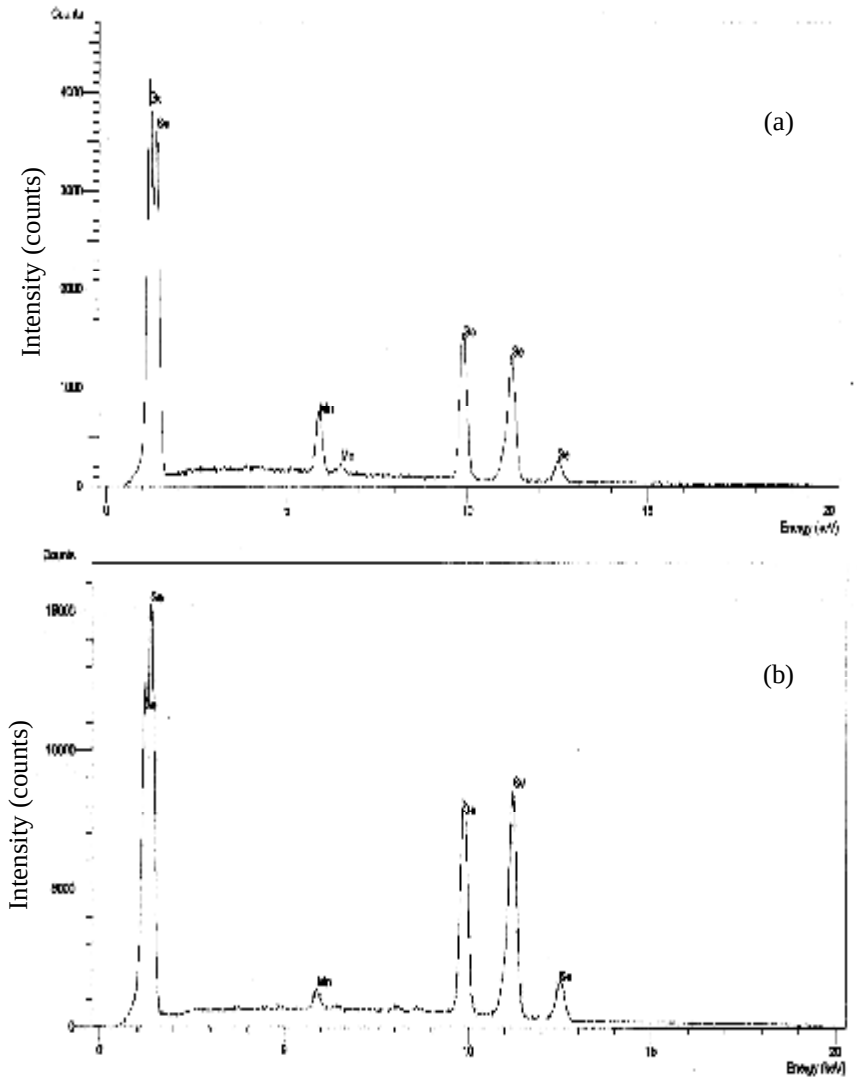

Fig. (1): The EDX spectrum of samples
(a) $Ge_{9.0}$ $Mn_{0.1}Se$ (b) $Ge_{0.8}Mn_{0.2}$ Se.

The detection of defects was carried out for the as-prepared samples by electron spin resonance (ESR). The ESR spectra were recorded at room temperature using Bruker EMX spectrometer (X-band) – Germany product

working at 9.677 GHz microwave frequency and 3.181 mw microwave power. All measurements previously mentioned were worked at the National Center for Radiation Research and Technology.

The magnetization M(H) as a function of the applied magnetic field H was determined at room temperature. The measurements were carried out using LakeShore 7410 magnetometer (VSM) with the applied field of 3.1 T. The VSM Unit at Nanotechnology Characterization Center (NCC), Agriculture Research Center (ARC), Cairo University was used.

3. Results and Discussion:

The structure of the as-prepared samples was investigated in wide range of Bragg's angle (10-80^o). Fig. (2) shows the X-ray diffraction patterns (XRDP) for the investigated samples. As shown, low intensity and broad diffraction lines are detected reflecting thus their amorphous texture. Applying Winfit program, the apparent grain size D_β (Å) and D_f (Å) and root mean square strain <eg> from single line analysis of $Ge_{1-x}Mn_xSe$ (x = 0.1 and 0.2) are given in Table (1). The obtained data show that the size of the grains ranges between 18 and 36 Å. However with Mn = 0.1, formation of small size crystallites in the range 12-15 nm are dominant. Such small crystallites disappeared as Mn was increased as it is seen in SEM photographs (Fig.(3)). The values of <eg> given in Table (1) shows also that the average strain increases with the increase of Mn. This means that disorder increased with increasing Mn content.

Table (1): Apparent crystallite size D_β (A^0) and D_f (A^0) and root mean square strain < eg > from single line analysis of $Ge_{1-x}Mn_xSe$ (x = 0.1, 0.2)

Sample	2θ	D_β (A^0)	D_f (A^0)	< eg >
$Ge_{0.9}Mn_{0.1}Se$	14.130	20	25	0.06051
	29.202	18	22	0.08472
	51.389	21	36	0.06901
	44.258	123	128	0.00187
	64.411	144	149	0.00206
	77.501	69	73	0.00203
Average		66	71	0.03675
Sample	2θ	D_β (A^0)	D_f (A^0)	< eg >
$Ge_{0.8}Mn_{0.2}Se$	14.687	24	26	0.10455
	28.277	18	23	0.06221
	50.827	26	31	0.10085
Average		23	27	0.08920

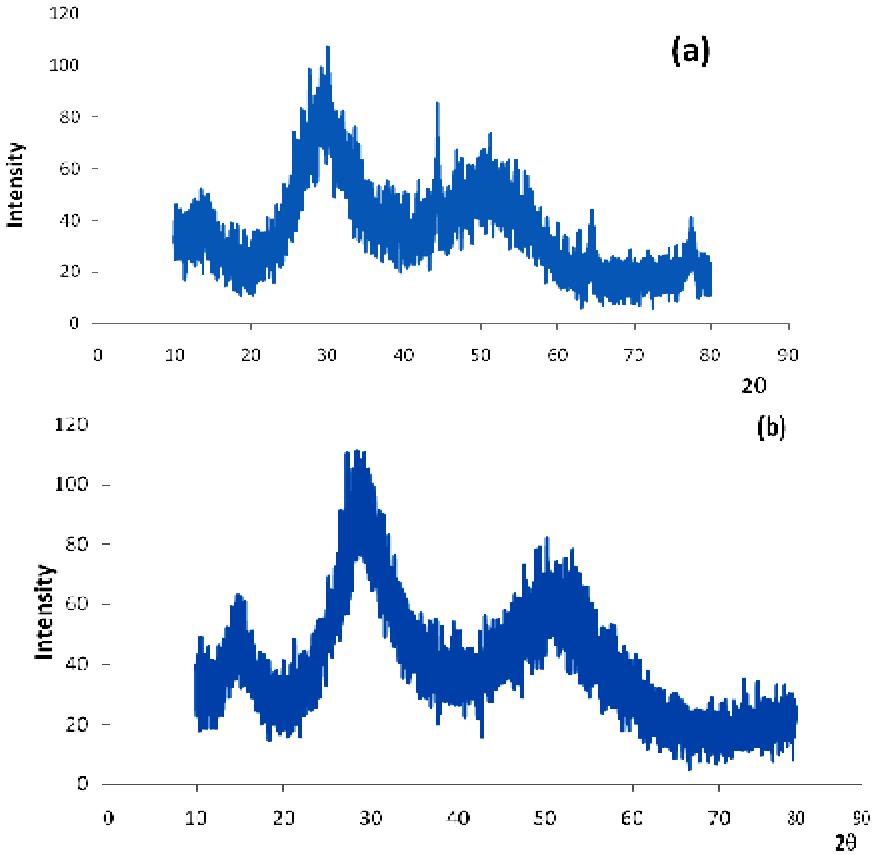

Fig. (2): X-ray diffraction for (a) $Ge_{9.0}$ $Mn_{0.1}Se$ (b) $Ge_{0.8}Mn_{0.2}$ Se.

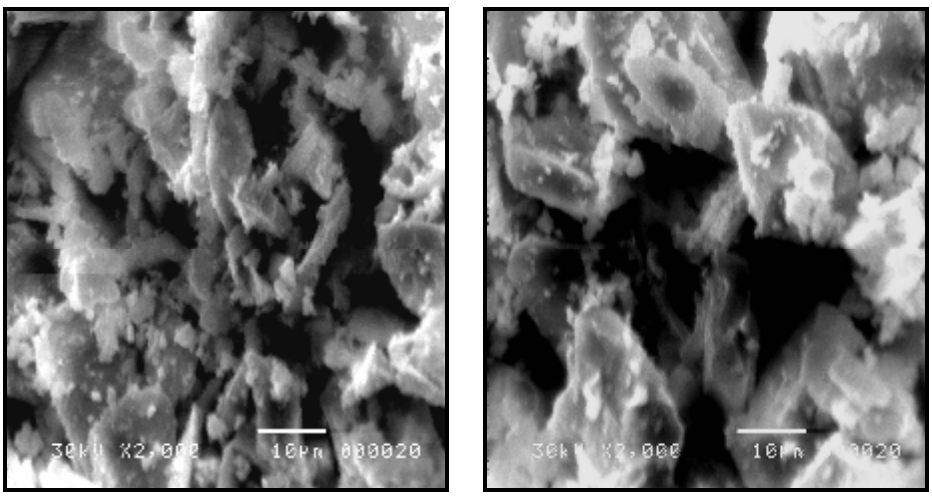

Fig. (3): The SEM images of samples (B) $Ge_{9.0}$ $Mn_{0.1}Se$ (b) $Ge_{0.8}Mn_{0.2}$ Se.

The temperature dependence of the dc conductivity (σ) for the investigated samples are plotted in Fig. (4) as a function of 10^3 /T. For $Ge_{0.9}Mn_{0.1}Se$ sample the plot indicates that there are two types of conduction mechanisms, according to one slope at a temperature range (300 – 335) and other slope at a temperature range (335 – 420), that contribute to the conductivity. For $Ge_{0.8}Mn_{0.2}Se$ sample the plot shows only one slope i.e. the presence of only one conduction mechanism over the whole range of temperature. The linearity of the function in the high temperature region shows that the conduction could be described by the Arrhenius relation [11]:

$$\sigma=\sigma_0 \exp (- \Delta E / K_B T) \qquad (1)$$

where σ_0 is the pre-exponential factor, ΔE is the activation energy of conduction and K_B is the Boltzman constant. The results of the electrical parameters are listed in Table (2). The data reveal that increasing Mn ratio produces an increase in the conductivity at room temperature $\sigma_{r.t}$ and a decrease in σ_0 and the activation energy of conduction. Following Mott and Davis [11] this decrease is due to the increase in density of localized states and consequently increase in carrier scattering by lattice imperfections. The high values of σ_0 argue conduction through carriers transfer between extended states in the valence and conduction bands according to Mott model for electronic conduction in amorphous materials.

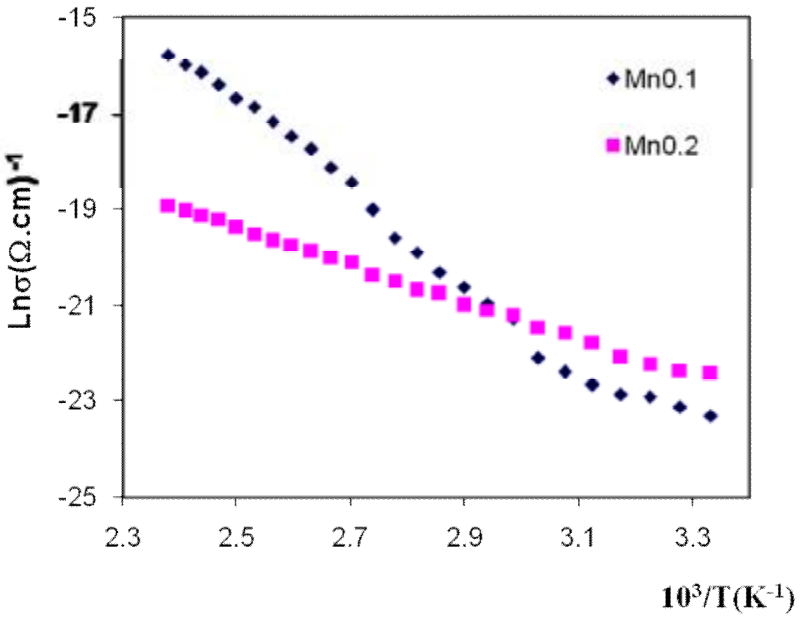

Fig. (4): The Dc conductivity Vs. reciprocal temperature for $Ge_{9.0}$ $Mn_{0.1}Se$ and $Ge_{0.8}Mn_{0.2}$ Se.

In material science, transition metals (like Mn) and rare earths because of their d and f bands are used as modifiers for S.C. as they can bond to the structure in a strongly covalent manner and yet create a variety of new electronic configurations through the interaction of their d or f electrons with their local environment forming multiple orbitals [10]. The result is that interactive transition-metal orbital configurations yield bands of electron states in the forbidden gap in different densities and energies. The reduced obtained value of the activation energy of (0.34 eV) suggests charge carrier transfer into these bands.

Table (2): Electrical Parameter of The Investigated Samples.

Composition	ΔE_1(eV)	ΔE_2(eV)	σ_0 $(\Omega.cm)^{-1}$	σ_{RT} $(\Omega.cm)^{-1}$
$Ge_{0.9}Mn_{0.1}Se$	0.83	0.32	14.99	7.69×10^{-11}
$Ge_{0.8}Mn_{0.2}Se$	0.34	-	0.03	1.57×10^{-10}

The AC conductivity $\sigma_{ac}(\omega)$ is obtained by subtracting the dc conductivity (σ_{dc}) from the measured total conductivity σ_{total} (ω) in accordance with [12]:-

$$\sigma_{ac}(\omega) = \sigma_{total}(\omega) - \sigma_{dc} \qquad (2)$$

The AC conductivity increases linearly with frequency according to the relaxation caused by the motion of electrons or atoms, tunneling or hopping between two equilibrium sites. Hence $\sigma_{ac}(\omega)$ can be written as:

$$\sigma_{ac}(\omega) = A\,\omega^{s} \qquad (3)$$

where the exponent s is near unity and, A is constant depending on temperature. Fig. (5) shows a typical experimental sets of Ln $\sigma_{ac}(\omega)$ as a function of temperature for the investigated samples at different frequencies for the two samples. The data shows that $\sigma_{ac}(\omega)$ is frequency dependent and almost temperature independent. The plot of log $\sigma_{ac}(\omega)$ versus log (ω) at different temperatures are displayed in Fig. (6). Obviously the plot reveals a good linear relation. The calculated S values as a function of temperature are shown in Fig. (7). This suggests that S is temperature almost independent. In this case the temperature dependence of ac conductivity for the investigated samples can be interpreted via the quantum mechanical tunneling (QMT). The ac conductivity for single electron motion undergoing QMT is expressed by the following relation [13]:

$$\sigma_{ac}(\omega) = [\, Be^2k_BT/\alpha \,]\, N^2(E_F)\omega\, R_\omega^{\,4}$$

where N (E_F) is the density of states at Fermi level, B is a numerical constant, α is the polarizability of a pair of sites and R_ω is the characteristic tunneling distance at a given frequency ω.

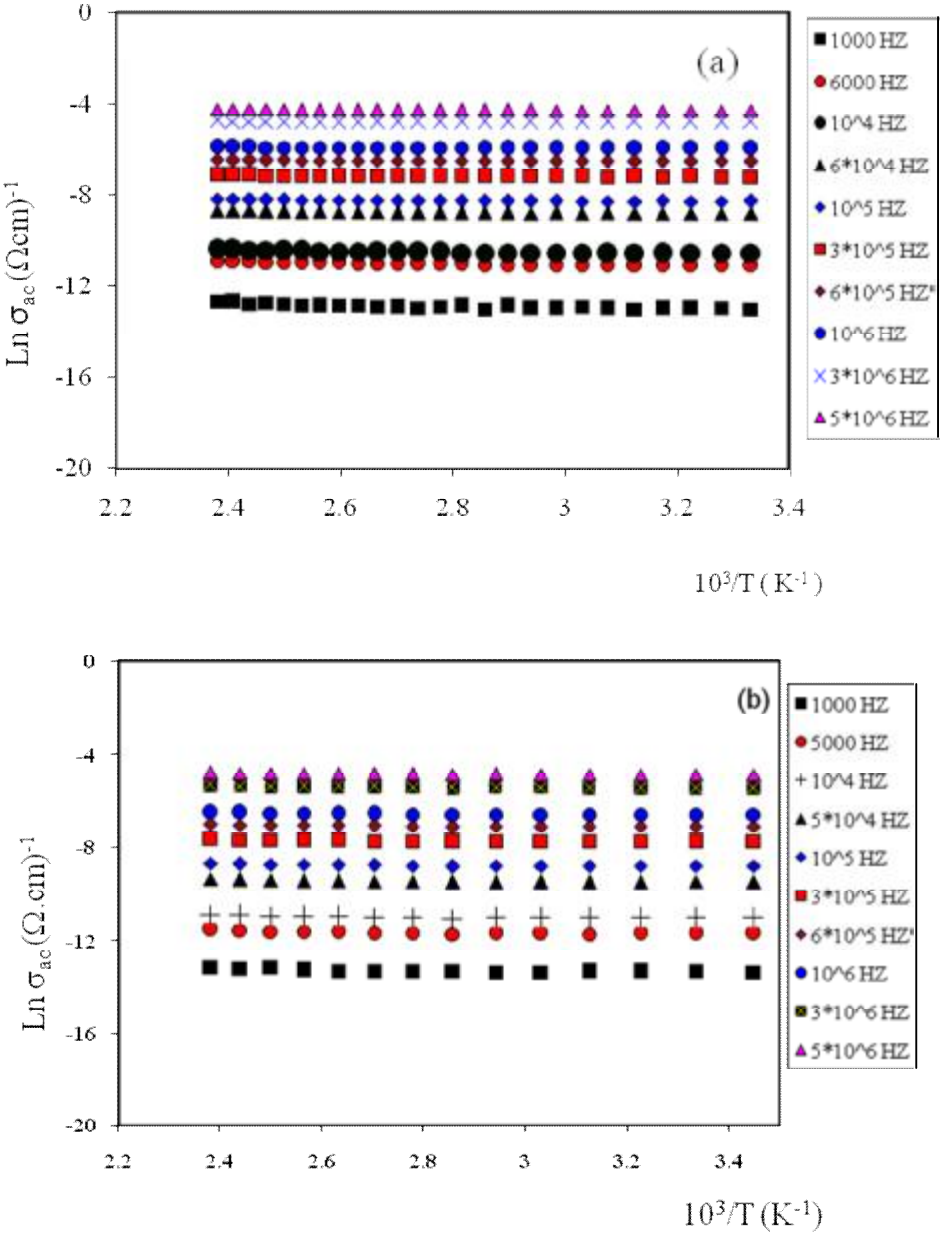

Fig. (5): The variation of the a. c. conductivity with reciprocal temperature for: (a) $Ge_{0.9}$ $Mn_{0.1}$ Se and (b) $Ge_{0.8}$ $Mn_{0.2}$Se.

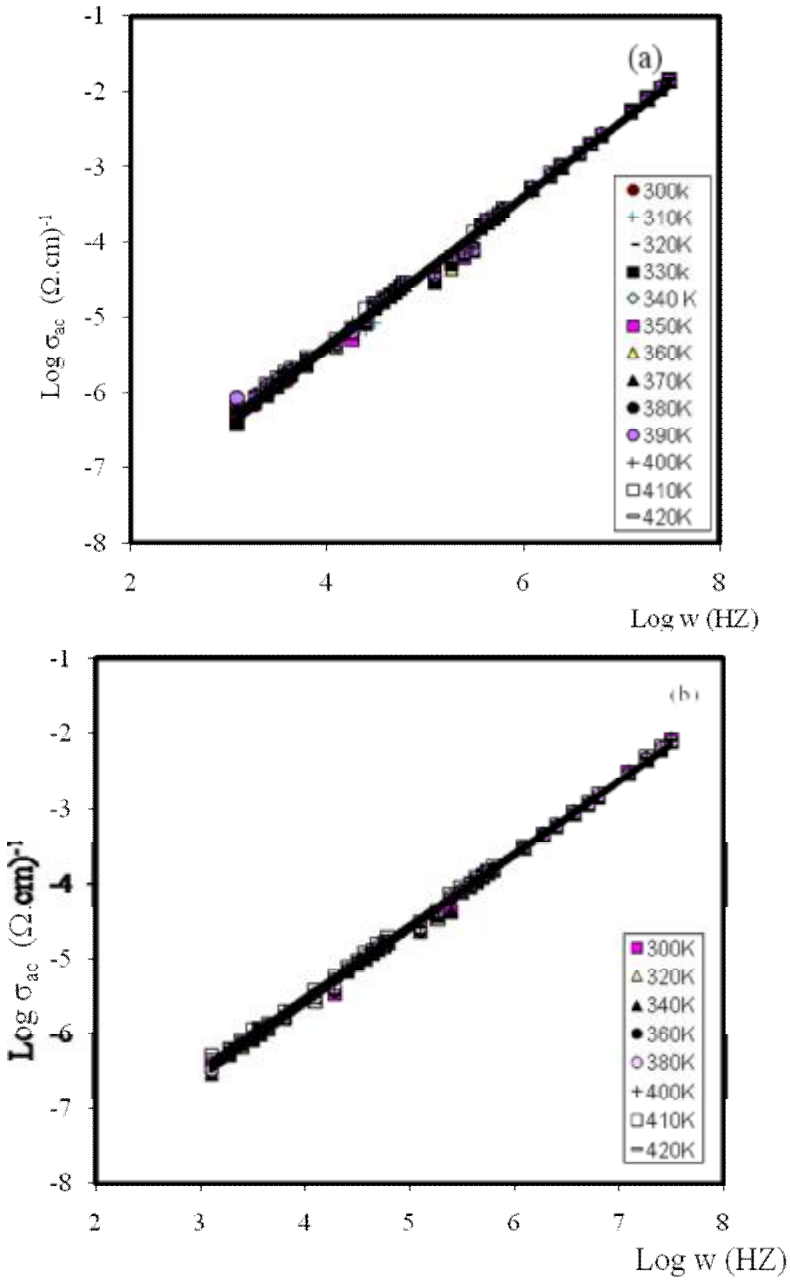

Fig. (6): Log a. c. conductivity VS. Log frequency for:
(a) $Ge_{0.9}$ $Mn_{0.1}$ Se and (b) $Ge_{0.8}$ $Mn_{0.2}$Se.

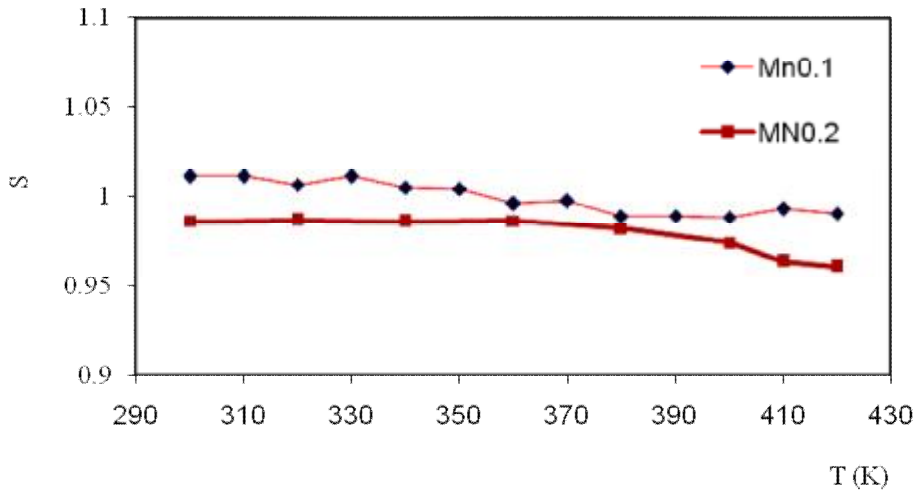

Fig. (7): Temperature dependence of the exponent s for $Ge_{9.0}$ $Mn_{0.1}Se$ and $Ge_{0.8}Mn_{0.2}$ Se.

The frequency exponent S is given by:

$$S = 1 - 4/\ln(1/\omega\tau_o)$$

where τ_o is the relaxation time.

The dielectric properties of a solid are very sensitive to the local distribution within the sample. The complex dielectric constant ε $(=\varepsilon' + i\varepsilon'')$ for the investigated samples was calculated according to the relation:

$$\varepsilon' = L/A\,(C/\varepsilon_0) \quad \text{and} \quad \varepsilon'' = \varepsilon' \tan\delta\,,$$

where C is the measured capacitance of the sample, ε_0 is the electric permittivity of free space (8.85×10^{-12} F/m) and $\tan\delta$ is the dielectric loss tangent, which was calculated from the phase angle (θ).

Figure (8) shows the temperature dependence of the dielectric constant ε' in the frequency range from 5×10^3 Hz to 10^6 MHz and temperature range from 300 – 420 K. The figure illustrates that ε' increases with increasing temperature and decreases with increasing frequency. This behavior can be attributed to the fact that at low frequencies and high temperatures ε' is due to the contribution of multi-components of polarizability (electronic, ionic, orientetional and interfacial polarizability) [14]. When the frequency is increased, the dipoles will no longer

be able to follow those of the field. As the frequency is further raised, the permanent dipoles, if present in the medium, will be completely unable to follow the field and the orientation polarization ceases. This consequently decrease the value of $\varepsilon^{/}$. At low temperatures, only the space charge (interfacial) polarization contributes to the polarization.

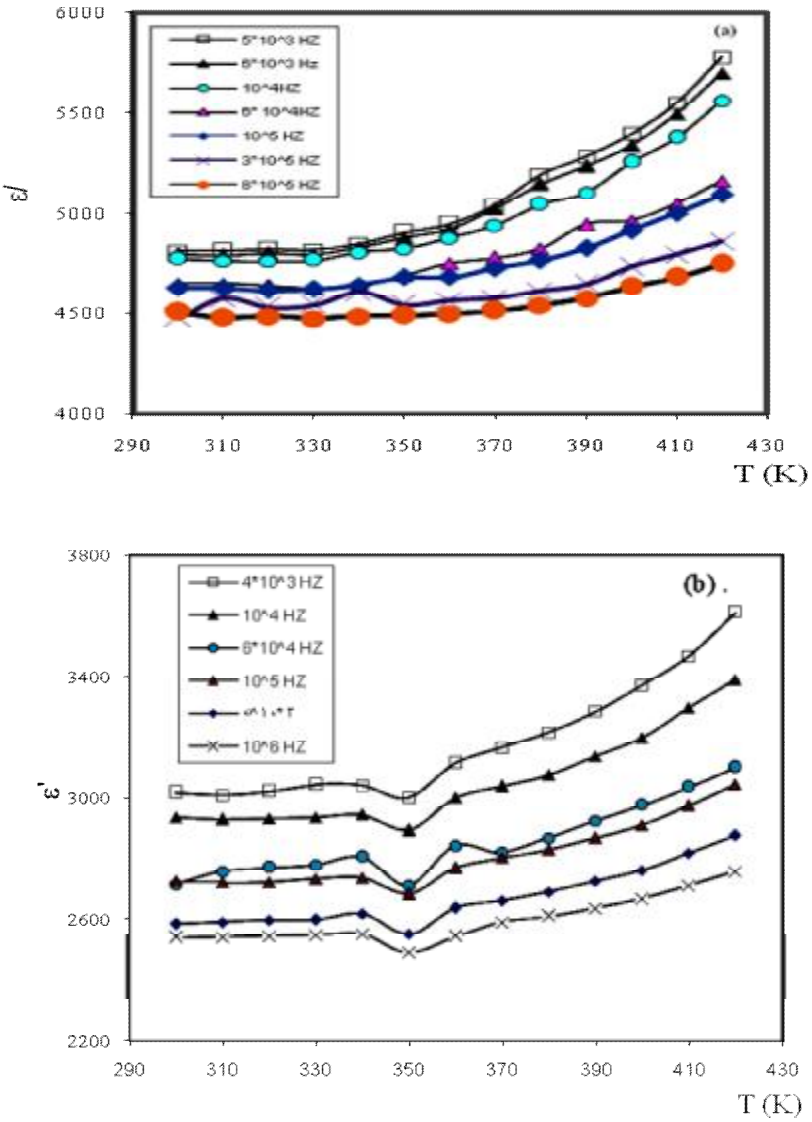

Fig.(8): The dielectric loss as a function of temperature for (a) $Ge_{9.0}$ $Mn_{0.1}Se$ and (b) $Ge_{0.8}Mn_{0.2}$ Se.

The frequency and temperature dependence of the dielectric loss $\varepsilon^{//}$ for the investigated samples is presented given in Fig.(9). The figure illustrates that $\varepsilon^{//}$ increases with increasing temperature and decreases with increasing frequency. The dependence of $\varepsilon^{//}$ with temperature and frequency was explained by Stevels [15], who divided the relaxation phenomena into three parts: conduction loss, dipole relaxation losses and deformation losses (vibration loss). These losses involve the migration of ions over large distances. This motion is the same as that occurring under direct current conditions. The ions jump over the highest barriers in the network. As the ions move, they give some of their energy to the lattice as a heat and amount of heat lost per cycle is proportional to (σ /ω).

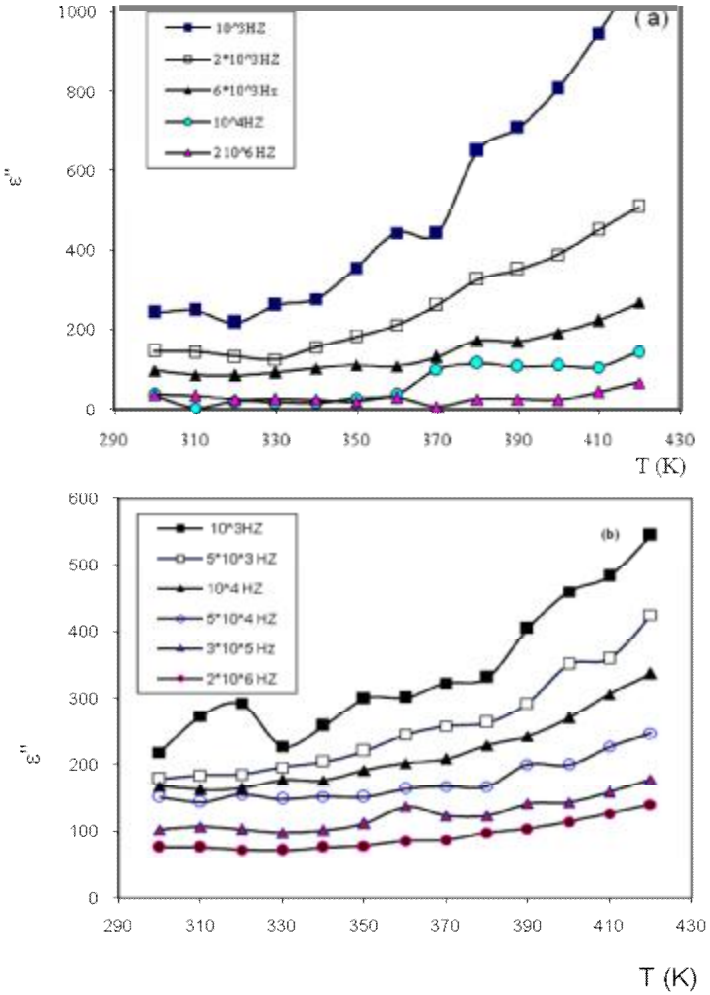

Fig.(9): The dielectric loss as a function of temperature for (b) $Ge_{0.9}$ $Mn_{0.1}Se$ and (b) $Ge_{0.8}Mn_{0.2}$ Se.

Figure (10) illustrates the magnetization as a function of the applied magnetic field of the investigated samples at room temperature. It is clear that $Ge_{0.9}Mn_{0.1}Se$ sample exhibits paramagnetic behavior. While for $Ge_{0.9}Mn_{0.2}Se$ sample the relation M-H gives a very narrow hysteresis loop which indicate the ferromagnetic exchange interaction between the magnetic ions. The coercive field H_c, remnant magnetization M_r, saturation magnetization M_s and susbitability χ at room temperature are listed in Table (3). Depending on the value of M_r we can define the suitable application for these materials. The low value of M_r means that $Ge_{0.9}Mn_{0.2}Se$ can be used as a transformer core.

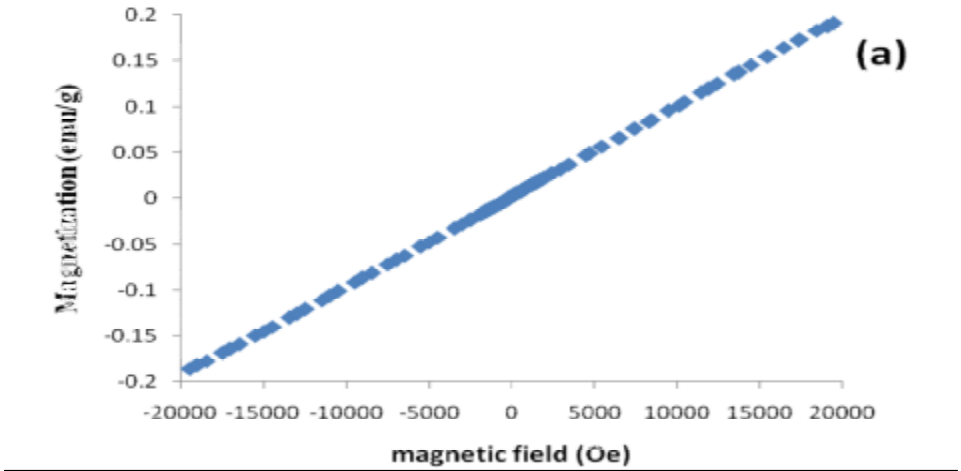

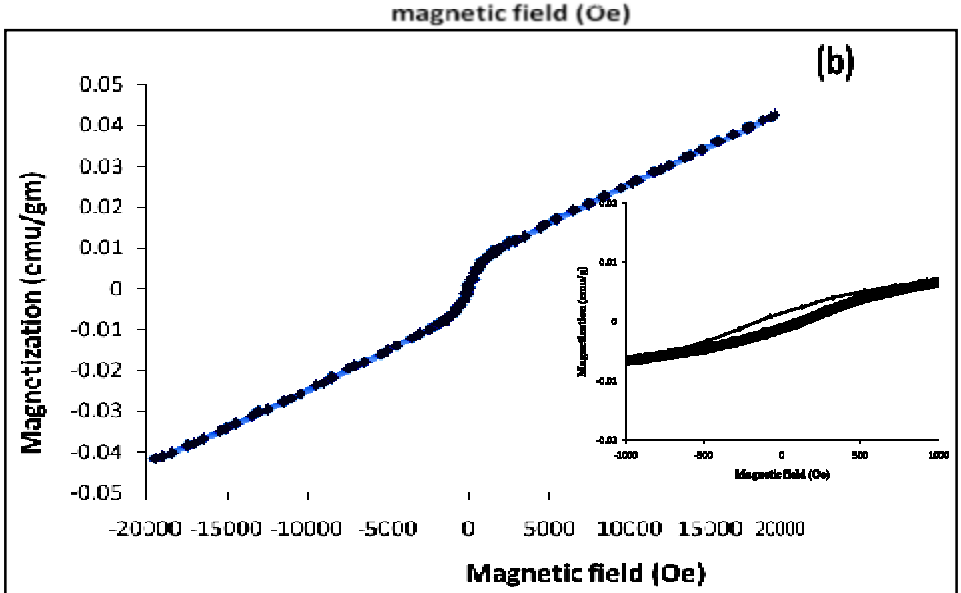

Fig.(10): Magnetization versus magnetic field at room temperture for (a) $Ge_{9.0}$ $Mn_{0.1}Se$ and (b) $Ge_{0.8}Mn_{0.2}$ Se.

Table (3): Values of saturation magnetization (Ms), Residual magnetization (Mr), Coerecivity (Hc) and Susbitabilty (χ) of the $Ge_{0.8}Mn_{0.2}Se$.

(Ms) emu/gm	(Mr) emu/gm	(Hc) G	(χ) (emu/gm)
0.042118	949.92×10^{-6}	104.21	12.138×10^{-6}

ESR spectroscopy is used in various branches of science for the detection and identification of free radicals and paramagnetic centers. Fig.(11) shows the corresponding ESR spectra for the investigated samples. As shown, a symmetric signal is detected for each of the investigated samples with g values equal to 2.00981and 2.00239, respectively. This allows to conclude the presence of free carriers. The concentration of free spin centers of the investigated samples (N) can be determined using the following relation:

$$N = P\ H_0\ (\Delta H)^2 (A/2) / G_e H_m\ (P_H)^{1/2}$$

where P is a constant of spectrum $\cong 9.1 \times 10^{12}$, H_0 is the magnetic field corresponding to the center of signal, ΔH is the width of the magnetic field from peak to peak, A is the height, G_e is the gain detection, H_m is the modulation field and P_H is the microwave power.

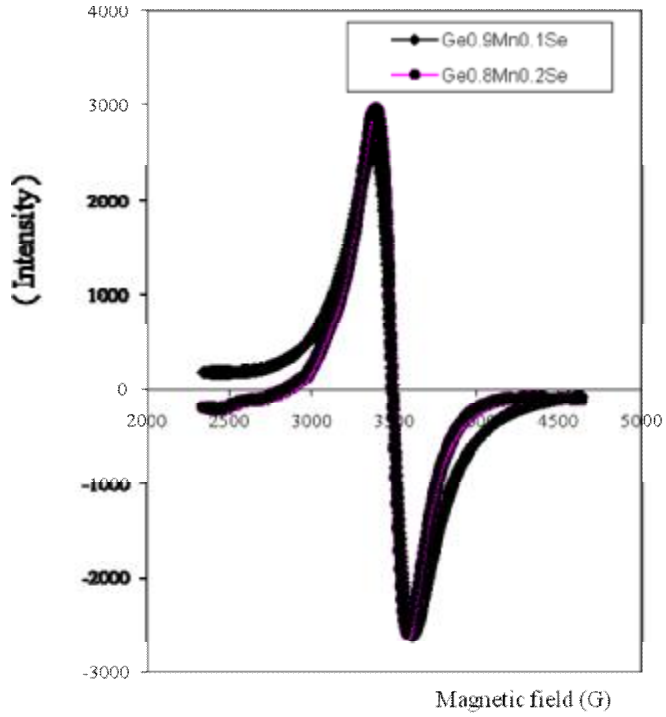

Fig. (11): ESR Spectra for the investigated samples.

The obtained densities of free spin centers are 9.12 x 10^{20} and 1.05 10^{22} cm^{-3} for $Ge_{0.9}Mn_{0.1}Se$ and $Ge_{0.8}Mn_{0.2}Se$ samples, respectively. The data illustrates that the number of paramagnetic defects increase with increasing Mn content.

4. Conclusion:

Amorphous $Ge_{1-x}Mn_xSe$ (x = 0.1 and 0.2) are characterized using X-ray diffraction, Ac and dc conductivity and ESR technique. X-ray study showed that the prepared samples have nano structure. The calculated grain size decreases with increasing Mn content. The decrease in the activation energy and pre-exponential factor with increasing Mn content means that the disorder and localized states density increased with increasing Mn content. The change of magnetic behavior from paramagnetic to ferromagnetic illustrates that changing Mn content affect deeply the magnetic properties.

Reference:

1. H. Ohno, *Science*, **281**, 951 (1998).
2. Dp. Divincenzo, *Science*, **270**, 255 (1995).
3. Y. Ohno, D.K. Young, B. Beschoten, F. Matsukura, H. Ohno and D. D. Awschalom, Nature, **281**, 790 (1999).
4. T. Hayashi, M.Shen, *J. Appl. Phys*., **390**, 949 (2000).
5. A. Van Esch, L. Van Bockstal, J. De Boeck., *Phys. Rev. B*, **56**, 13103 (1997).
6. H. AKinaga, J. De Boeck, G. Borghs, *Appl. Phys. Lett*., **72**, 3368 (1998).
7. P. J. Wellmann, J.M. Garcia, J. L. Feng, P.M. Petroff, *Appl. Phys. Lett*,
8. **71**, 2532 (1997).
9. J. H. Kim, D. Kim, Y. E. Ihm, and W. K. Choo, *J. Appl. Phys*., **92**, 6066 (2002).
10. Y.M. Cho, W. K. Choo, H. Kim, D. Kim, and Y. Ihm, *Appl. Phys. Lett*., **80**, 3358 (2002).
11. Tianhao Ji, wen – Bin Jian, Jige Fang, Jinke Tang, Volodymy colub, and Leonard Spina, *IEEE Transactions Magnetics*, **39**, 2791 (2003).
12. N.F. Mott and E.A. Davis, *Electronic Processes in Non-Crystalline Materials, Clarendon Press. Oxford*, P.200 (1971).
13. K. Sharma and K.L. Bahata, *J. Non-Cryst. Solids*, 95 (1989).
14. A. Ghosh, *Phys. Rev*., **B41**, 1479 (1990).
15. Glass, 1977 Volume I, Edited by J. Gotz.
16. J.M. Stevels, *The electrical properties of glass*, P. 350 (1975).